-Extended Pyrene-Fused Double [7]Carbohelicene as a Chiral Polycyclic Aromatic Hydrocarbon

JACS JOURNAL OF THE AMERICAN CHEMICAL SOCIETY

Article

Cite This: J. Am. Chem. Soc. 2019, 141, 12797−12803

pubs.acs.org/JACS

π-Extended Pyrene-Fused Double [7]Carbohelicene as a Chiral Polycyclic Aromatic Hydrocarbon

Yunbin Hu,[†,‡] Giuseppe M. Paternò,[§] Xiao-Ye Wang,[†] Xin-Chang Wang,[∥] Michele Guizzardi,[⊥] Qiang Chen,[†] Dieter Schollmeyer,[#] Xiao-Yu Cao,[∥] Giulio Cerullo,[⊥] Francesco Scotognella,[§,⊥] Klaus Müllen,*[,†,▽] and Akimitsu Narita*[,†,■]

[†]Max-Planck-Institut für Polymerforschung, Ackermannweg 10, Mainz 55128, Germany

[‡]Department of Organic and Polymer Chemistry, College of Chemistry and Chemical Engineering, Central South University, Changsha, Hunan 410083, People's Republic of China

[§]Center for Nano Science and Technology, Istituto Italiano di Tecnologia, Milano 20133, Italy

[∥]Department of Chemistry and Chemical Engineering, Xiamen University, Xiamen 361005, China

[⊥]IFN-CNR, Department of Physics, Politecnico di Milano, Milano 20133, Italy

[#]Institut of Organic Chemistry, Johannes Gutenberg-University Mainz, Duesbergweg 10-14, Mainz 55099, Germany

[▽]Institute of Physical Chemistry, Johannes Gutenberg-University Mainz, Duesbergweg 10-14, Mainz D-55128, Germany

[■]Organic and Carbon Nanomaterials Unit, Okinawa Institute of Science and Technology Graduate University, 1919-1 Tancha, Onna-son, Kunigami, Okinawa 904-0495, Japan

Supporting Information

ABSTRACT: A π-extended double [7]carbohelicene **2** with fused pyrene units was synthesized, revealing considerable intra- and intermolecular π−π interactions as confirmed with X-ray crystallography. As compared to the previous double [7]carbohelicene **1**, the π-extended homologue **2** demonstrated considerably red-shifted absorption with an onset at 645 nm (**1**: 550 nm) corresponding to a smaller optical gap of 1.90 eV (**1**: 2.25 eV). A broad near-infrared emission from 600 to 900 nm with a large Stokes shift of ∼100 nm (2.3 × 10^3 cm^{-1}) was recorded for **2**, implying formation of an intramolecular excimer upon excitation, which was corroborated with femtosecond transient absorption spectroscopy. Moreover, **2** revealed remarkable chiral stability with a fairly high isomerization barrier of 46 kcal mol^{-1}, according to density functional theory calculations, which allowed optical resolution by chiral HPLC and suggests potential applications in chiroptical devices.

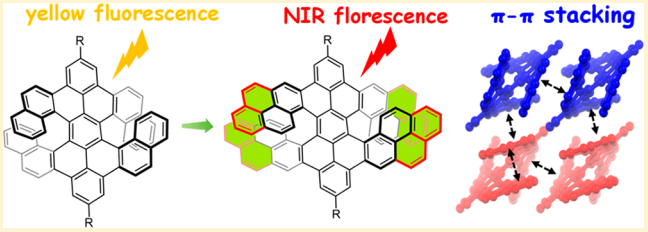

INTRODUCTION

Nonplanar polycyclic aromatic hydrocarbons (PAHs) have attracted growing interest during the past decade, due to their unique optoelectronic properties, conformational dynamics, and intriguing supramolecular characteristics, distinct from those of planar PAHs.[1−4] Moreover, chirality can be induced in nonplanar PAH structures when both an inversion center and a mirror plane are absent,[5] paving the way for the emerging field of chiral photonics and electronics.[6−10] Chiral PAHs, with emission in the red to near-infrared (NIR) region (emission wavelength > 700 nm), are especially interesting, for example, with potential applications for in vivo bioimaging and NIR light-emitting devices,[11−14] employing circularly polarized luminescence. More interestingly, chiral π-conjugated system-based field-effect transistor can be utilized to detect the circularly polarized lights, which is inherently difficult with conventional photodetectors based on nonchiral semiconductors.[15] To achieve a high sensitivity in such photodector, high charge-carrier mobility is crucial, where efficient π−π stacking of semiconducting materials plays an important role. However, twisting of π-systems often disturbs intramolecular π-conjugation and intermolecular π−π stacking interactions, which can be detrimental for achieving NIR optical responses and efficient intermolecular charge/electron transfer that are important for the aforementioned future applicaitons.[16−18] To this end, it is highly desirable to develop nonplanar PAHs with NIR photoluminescence and pronounced intermolecular π−π interactions, which are still underexplored.[19−21]

Helicenes, consisting of consecutive *ortho*-condensed aromatic rings, are among the most studied nonplanar chiral PAHs.[22−24] Considerable effort has been devoted to the development of new synthetic methods for forming helicene (sub)structures and to the achievement of higher helicenes,[23−25] with [16]helicene reported by Fujita and co-workers as the record to date.[26] Nevertheless, *ortho*-fusion of

Received: May 29, 2019
Published: July 22, 2019

DOI: 10.1021/jacs.9b05610
J. Am. Chem. Soc. 2019, 141, 12797−12803

an increasing number of benzene rings in pristine helicenes has little effect on the optical absorption and energy gap when higher than [5]helicene.[27−30] To this end, π-extension of helicenes, which can significantly modulate their optical and electronic properties, has been attracting increased attention recently.[31−34] In 2018, Hirose and Matsuda et al. reported a hexabenzo-fused [7]helicene (**B**, Figure 1a), exhibiting a

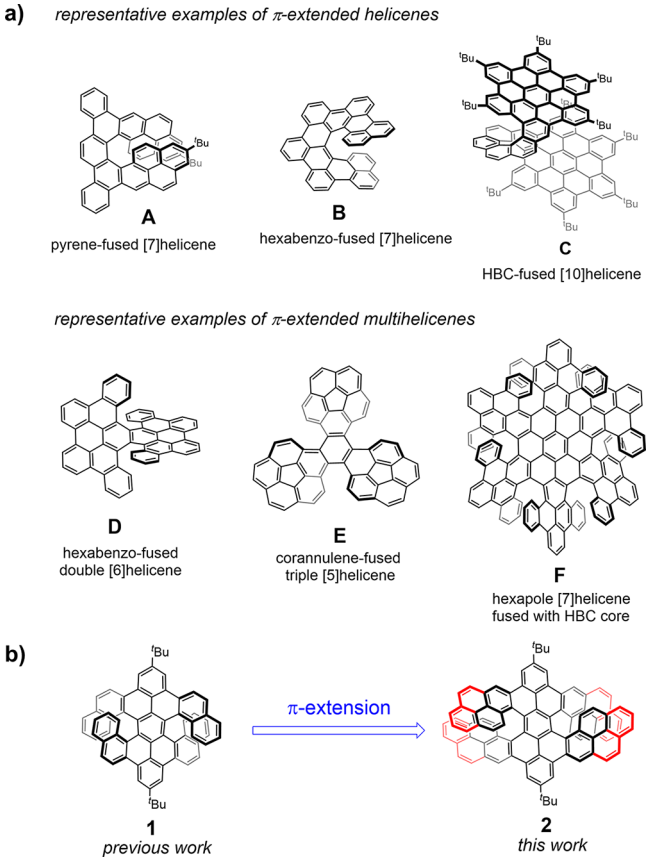

Figure 1. (a) Representative examples of π-extended helicenes and multihelicenes. (b) Extension of dibenzo-fused double [7]-carbohelicene **1** to double [7]carbohelicene **2** with fused pyrene units.

largely red-shifted absorption and a narrowed optical gap relative to its parent [7]helicene.[32] Martín and co-workers have demonstrated the synthesis of a [10]helicene fused with two hexa-*peri*-hexabenzocoronene (HBC) units (**C**, Figure 1a), showing multiple redox activity.[34] In addition, π-extension can also promote π−π interactions of pristine helicenes, and both **A** and **C** have exhibited enhanced intramolecular π−π interactions as compared to their parent helicenes (Figure 1a).[32,34] Nevertheless, helicenes with strong intermolecular π−π interactions have remained elusive.

In addition to conventional helicenes, double and multiple helicenes, entailing more than one helicene subunit in one molecule, have emerged as a new class of chiral PAHs. Double and multiple helicenes reveal enhanced chiroptical responses and unique self-assembling characteristics that are distinct from those of single helicenes.[35] There is an increasing number of π-extended multihelicenes reported in the literature,[36−39] as exemplified by the π-extended double [6]helicene (**D**, Figure 1a),[36] corannulene-fused triple [5]helicene (**E**, Figure 1a),[37] and hexapole [7]helicenes fused to an HBC core (**F**, Figure 1a),[38] which reveal structures with unique crystal packing motifs and/or broadened optical absorption. However, multihelicenes with efficient intra- and intermolecular π−π interactions have rarely been reported, and thus far there are only a few examples of helicenes and multihelicenes with NIR emission at >700 nm.[39]

To this end, we considered possible π-extension of the benzo-fused double [7]carbohelicene **1** that we have previously reported (Figure 1b).[40] Here, we report the synthesis and characterization of double [7]carbohelicene **2** with fused pyrene subunits, which can be regarded as a π-extended homologue of **1**. Direct comparison of **1** and **2** clearly revealed the effect of the π-extension on the optical and electronic properties of **1**. Substantial intra- and intermolecular π−π interactions could be observed in the crystal structure of **2**, in contrast to the absence of π-stacking in crystals of **1**. Moreover, broad NIR emission of **2** was recorded from 600 to 900 nm, which could be ascribed to an intramolecular excimeric state, as demonstrated with femtosecond transient absorption (TA) spectroscopy.

RESULTS AND DISCUSSION

Synthesis of Pyrene-Fused Double [7]Carbohelicene. Synthesis of the laterally extended double helicene **2** was accomplished in two steps, starting from the known tetrabromoterphenyl **3** (Scheme 1).[40] First, **3** was subjected

Scheme 1. Synthesis of Pyrene-Fused Double [7]Carbohelicene 2

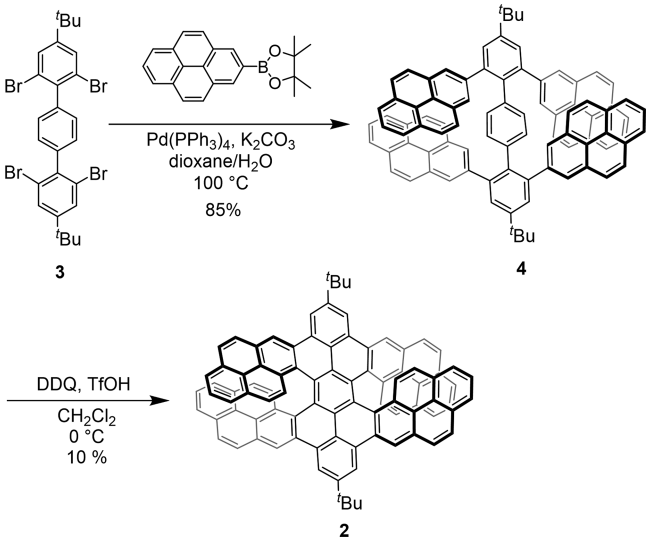

to a 4-fold Suzuki-coupling reaction with pyrene-2-bronic ester, catalyzed by tetrakis(triphenylphosphine) palladium(0) with potassium carbonate as the base, providing 2,2′′,6,6′′-tetrapyrenyl-4,4′′-di-*tert*-butyl-1,1′:4′,1′′-terphenyl (**4**) in 85% yield. Scholl-type intramolecular oxidative cyclodehydrogenation of precursor **4** was subsequently performed in the presence of 2,3-dichloro-5,6-dicyano-1,4-benzoquinone (DDQ) and triflic acid (TfOH), affording the target π-extended double helicene **2** in 10% yield. The low yield of **2**, in comparison to the case of **1** (76%), is presumably due to higher steric hindrance. Side products were insoluble and could not be identified. Double helicene **2** was fully characterized by high-resolution mass spectrometry and NMR spectroscopies (^{1}H NMR, ^{13}C NMR, ^{1}H−^{1}H COSY,

DOI: 10.1021/jacs.9b05610
J. Am. Chem. Soc. 2019, 141, 12797−12803

and $^{1}H-^{1}H$ NOESY; see the Supporting Information for further details).

Single-Crystal X-ray Analysis. To further reveal the structure of **2**, single crystals suitable for X-ray analysis were grown by slow diffusion of hexane vapor into a solution of **2** in carbon disulfide (Figure 2a). The structure of **2** with two π-extended double [7]helicene subunits was unambiguously demonstrated with two pairs of significantly overlapping terminal benzene rings (A/G and H/K) in each helix. Torsions defined by the dihedral angles for 7−2−3−8 and 9−5−6−10 are 20.9° and 21.9°, respectively, which are much smaller than those of double helicene **1** (28.5° and 30.6°).[26] Considering the absence of electron donor/acceptor moieties, the compressed double helical structure of **2** is likely caused by enhanced $\pi-\pi$ interactions between the π-extended terminal rings, analogous to previous π-extended helicenes in the literature.[32−35] The mean vertical distance between terminal rings A and G, defined as the average of the distance from the centroid of ring A to the plane of ring G and that from the centroid of ring G to the plane of ring A, is 3.26 Å (Figure 2b). This is significantly shorter than that of **1** (3.61 Å) and even smaller than the typical intermolecular $\pi-\pi$ stacking distance of planar PAHs such as HBC (3.42 Å) and benzodicoronene (3.46 Å),[41] reflecting significant intramolecular $\pi-\pi$ interactions. Additionally, the maximum torsion angle of the central benzene ring D was 29.8° (1−6−5−4), in comparison to 33.8° in **1**, indicating relatively decreased geometric distortion of the whole molecule **2**. One unit cell in the crystal packing consists of a pair of enantiomers **2**-(*P*,*P*) and **2**-(*M*,*M*), which display well-established intermolecular $\pi-\pi$ stacking, homochiral molecular packing along the *a*-axis with a mean vertical distance of 3.48 Å, and heterochiral packing along the *b*-axis with a distance of 3.42 Å (Figure 2c).

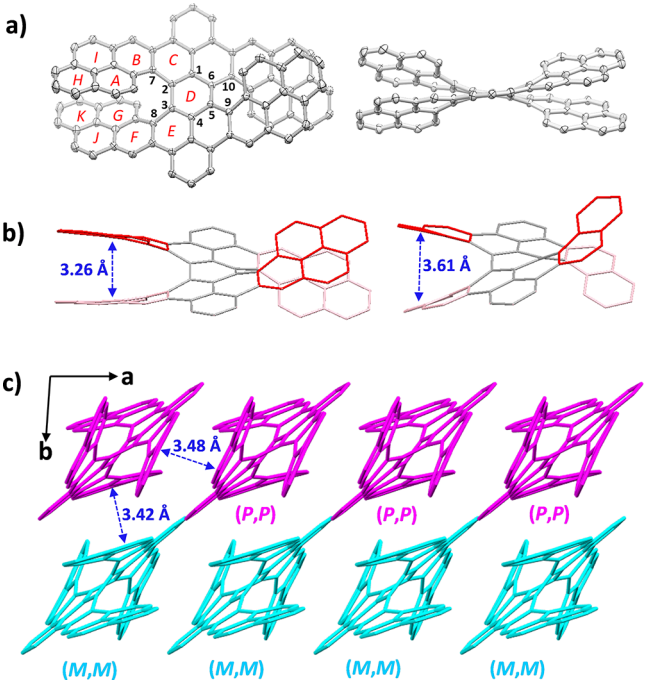

Figure 2. Crystal structure of pyrene-fused double [7]carbohelicene **2**. *tert*-Butyl groups and hydrogen atoms are omitted for clarity. (a) Top and side views of the ORTEP drawing of **2**, providing 50% probability thermal ellipsoids. (b) Comparison between crystal structures of **2** (left) and **1** (right), showing vertical distances between terminal benzene rings. (c) Crystal packing of **2**, showing homochiral stacking ($\pi-\pi$ stacking between molecules with the same handedness) along the *a*-axis and heterochiral stacking ($\pi-\pi$ stacking between molecules with different handedness) along the *b*-axis.

Optical and Electronic Properties. Optical properties of **2** were evaluated by UV−vis absorption and emission spectroscopy (Figure 3a). In comparison with double [7]-helicene **1**, the laterally extended homologue **2** exhibited a generally red-shifted absorption profile with an enhanced molar extinction coefficient ($\varepsilon_{max,1}$ = 1.0 × 10^5 L mol^{-1} cm^{-1} versus $\varepsilon_{max,2}$ = 2.2 × 10^5 L mol^{-1} cm^{-1}). The absorption spectrum of **2** featured three strong bands at 269, 379, and 449 nm, as well as a weak, low-energy band at 537 nm and a tail extending to 645 nm. On the basis of time-dependent density functional theory (TD-DFT) calculations, the low-energy absorption tail from 570 to 645 nm was attributed to the HOMO → LUMO transition (f = 0.066, λ_{calc} = 610 nm), while the bands at 537 and 449 nm were both assigned to a combined contribution of HOMO−1 → LUMO and HOMO → LUMO+1 transitions (f = 0.157, λ_{calc} = 549 nm/f = 1.003, λ_{calc} = 474 nm). The long-wavelength absorption onset of **2** is 645 nm, corresponding to an optical gap of 1.92 eV, which is

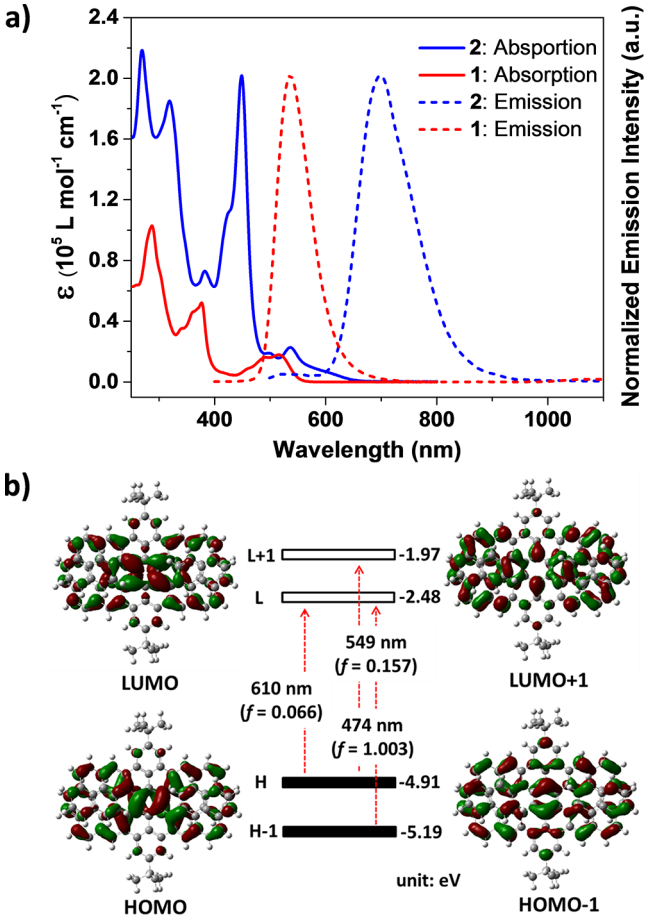

Figure 3. (a) Absorption (solid lines) and emission (dashed lines) spectra of **1** (7.48 × 10^{-6} mol L^{-1}, excitation wavelength: 376 nm) and **2** (6.43 × 10^{-6} mol L^{-1}, excitation wavelength: 450 nm) in dichloromethane. (b) Energy diagrams and major transitions between frontier orbitals of **2** calculated by TD-DFT at the B3LYP/6-311G(d,p) level of theory. Values in parentheses represent the oscillator strengths (f).

DOI: 10.1021/jacs.9b05610
J. Am. Chem. Soc. 2019, 141, 12797−12803

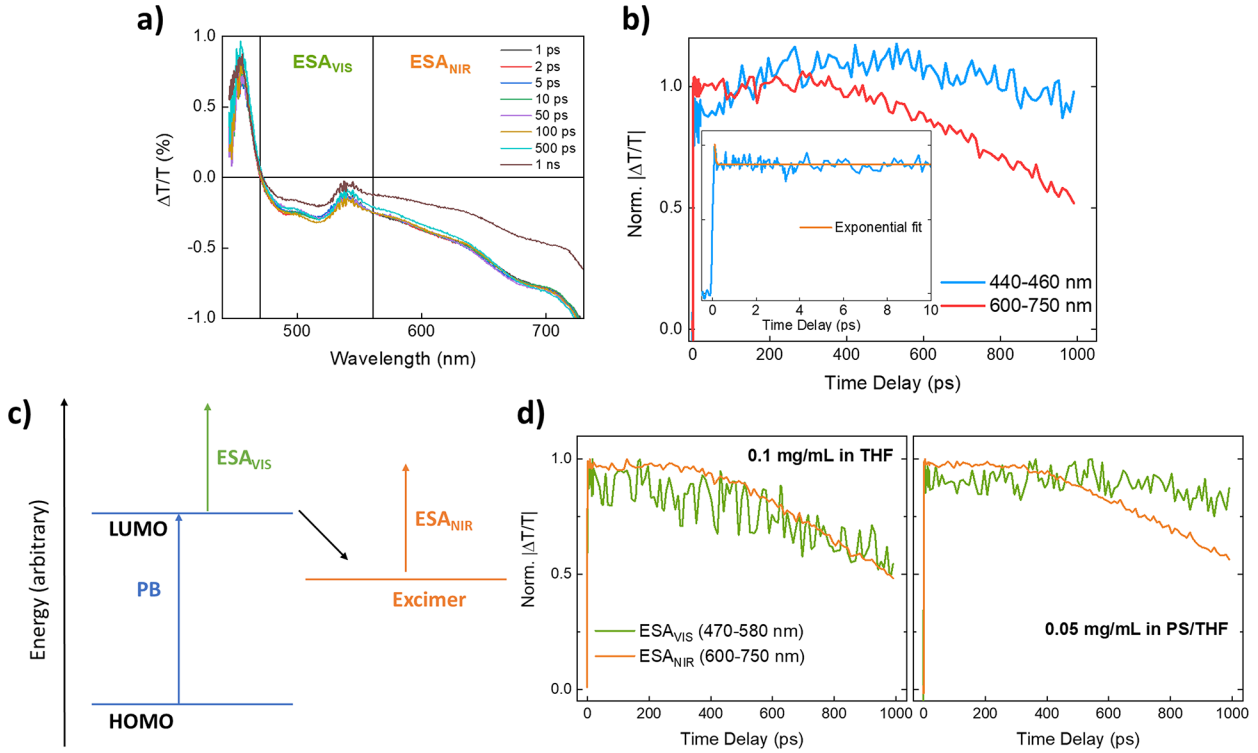

Figure 4. (a) Differential transmission ($\Delta T/T$) spectra of **2** at a pump–probe delay of 1 ps and (b) normalized $\Delta T/T$ dynamics (expressed in absolute value) of **2** in THF solution with the concentration of 0.1 mg/mL. The inset shows the first 10 ps of the dynamics, highlighting the ultrafast decay of the PB signal and the concomitant rise of the ESA (600–750 nm) trace. (c) Simplified scheme (not in absolute energy scale) showing the possible excited-state photophysics of **2** upon excitation with a pump pulse (530 nm). (d) Normalized $\Delta T/T$ dynamics (expressed in absolute value) of **2** in THF solution with the concentration of 0.1 mg/mL, and in 40 mg/mL polystyrene (PS) solution in THF with the concentration of 0.05 mg/mL.

lower than that of **1** (2.25 eV), reflecting the extended π-conjugation. On the other hand, **2** displayed a broad NIR fluorescence band between 600 and 900 nm, peaking at 697 nm, with a large Stokes shift of approximately 100 nm (2.3×10^3 cm^{-1}), in contrast to a small Stokes shift observed for **1** (20 nm, 7.3×10^2 cm^{-1}). To the best of our knowledge, this emission of **2** at around 700 nm is thus far one of the longest-wavelength emissions among the reported double and multiple carbohelicenes.[36,39,40,42] Although aggregation-induced fluorescence quenching was observed at a concentration of 10^{-4} M, the shape and emission maximum of fluorescence spectra did not change at lower concentrations, that is, from 10^{-7} to 10^{-5} M, suggesting that the red-shifted broad emission is not due to aggregation effects (Figure S5). These fluorescence properties might suggest the formation of an intramolecular excimer state upon excitation within the molecule of **2**, which is further supported by transient absorption studies described below. As indicated by the aforementioned crystallographic analysis, the intramolecular excimer can be stabilized by the closely stacked terminal pyrene subunits. These emission and structural properties have also been observed for a π-extended [7]helicene with fused pyrene moieties (**A**, Figure 1) giving stabilized intramolecular excimer states.[31] Cyclic voltammetry of **2** revealed two reversible oxidation processes with half-wave potentials at 0.68 and 0.92 V, as well as two reversible reduction curves with half-wave potentials at −1.43 and −1.61 V, respectively (Figure S6). Accordingly, the HOMO and LUMO energies were estimated to be −5.02 and −2.91 eV, respectively, corresponding to an electrochemical HOMO–LUMO gap of 2.11 eV, in good agreement with the DFT calculation (2.43 eV).

Transient Absorption Analysis. Ultrafast TA spectroscopy has proven to be an ideal tool to investigate the ability of nanographene molecules to establish pronounced intermolecular interactions.[43−45] Here, an ultrashort pump pulse (530 nm) allows one to populate the excited states, while a time-delayed broadband probe pulse (450–750 nm) interrogates both the differential transmission ($\Delta T/T$) spectra and the dynamics of those states on the femtosecond–picosecond time scale. The $\Delta T/T$ spectrum of double helicene **2** in a 0.1 mg/mL THF solution (Figure 4a) consists of a positive peak at 450 nm due to pump-induced ground-state depletion (photobleaching, PB) and a broad negative feature linked to excited-state absorption (ESA). On the basis of steady-state absorption data, we can subdivide such a broad ESA band into two contributions: (i) the signal in the visible (ESA$_{VIS}$, 470–550 nm) can be attributed to a transition of an excited electron from the LUMO to a higher lying excited state; and (ii) ESA in the red/near-infrared part of the spectrum (ESA$_{NIR}$, 600–750 nm) can be tentatively ascribed to absorption from the excimer state (Figure 4c).[46] The signature of a positive stimulated emission signal overlapping with the strong ESA$_{NIR}$ can also be seen at 700 nm. When comparing $\Delta T/T$ dynamics at probe wavelengths corresponding to the PB (440–460 nm) and the ESA$_{NIR}$ (600–750 nm) (Figure 4b), the former exhibits a first rapid decay with a time constant within our instrumental resolution (~150 fs, see inset of Figure 4b) and long growth (until ~280 ps), while the latter remains stable until 280–300 ps before decaying (estimated τ = 1 ns). These data

DOI: 10.1021/jacs.9b05610
J. Am. Chem. Soc. 2019, 141, 12797−12803

corroborate the excimer scenario, as the ultrafast PB decay can be related to the population of the energetically lower-lying excimer state (see Figure 4c), while the PB signal growth can be attributed to the "trapping" of the photogenerated species in such a relatively long-living state.[46,47] This is, in fact, another mechanism that additionally bleaches the ground level. Finally, to assess the effect of intermolecular interactions on ESA dynamics, we carried out TA measurements on a diluted solution of **2** (0.05 mg/mL) mixed with polystyrene (PS) (40 mg/mL) in THF (Figure 4d). In this case, the polymer acts as a molecular spacer, minimizing supramolecular contacts between the double helicene molecules. Whereas the ESA_{VIS} and ESA_{NIR} of **2** in THF feature virtually identical $\Delta T/T$ dynamics, in PS/THF ESA_{VIS} dynamics differ markedly from ESA_{NIR}, as the former displays a long-lived signal when compared to the relatively faster ESA_{NIR}. This result suggests that dilution in PS allows clear discrimination between the two states, with ESA_{VIS} possessing an intermolecular character and ESA_{NIR} with almost no dependency on dilution. Taken together, these data indicate that such ESA_{NIR} is, in fact, assignable to an intramolecular state, that is, an excimer, which is ultimately responsible for the broad and red-shifted emission observed in the steady-state fluorescence spectrum.

Chiroptical Properties. The isomerization process from (*P*,*P*)-**2** to its meso conformer (*P*,*M*)-**2** through a proposed transition state (TS) was predicted by DFT calculation at the B3LYP/6-311G(d,p) level of theory (Figure 5a). A high isomerization barrier of 46.3 kcal mol^{-1} was achieved, pointing toward the pronounced conformational and chiral stability of **2**, and enabling further optical resolution with the help of chiral high-performance liquid chromatography (HPLC). The two fractions were separated by chiral HPLC on a Daicel Chiralpak IE column, which displayed mirror-symmetric circular dichroism (CD) spectra, indicating a pair of enantiomers with opposite helicity. By comparing experimental and simulated CD spectra, absolute configurations of the two enantiomers, (*P*,*P*)-**2** and (*M*,*M*)-**2**, were clearly determined (Figure 5b).

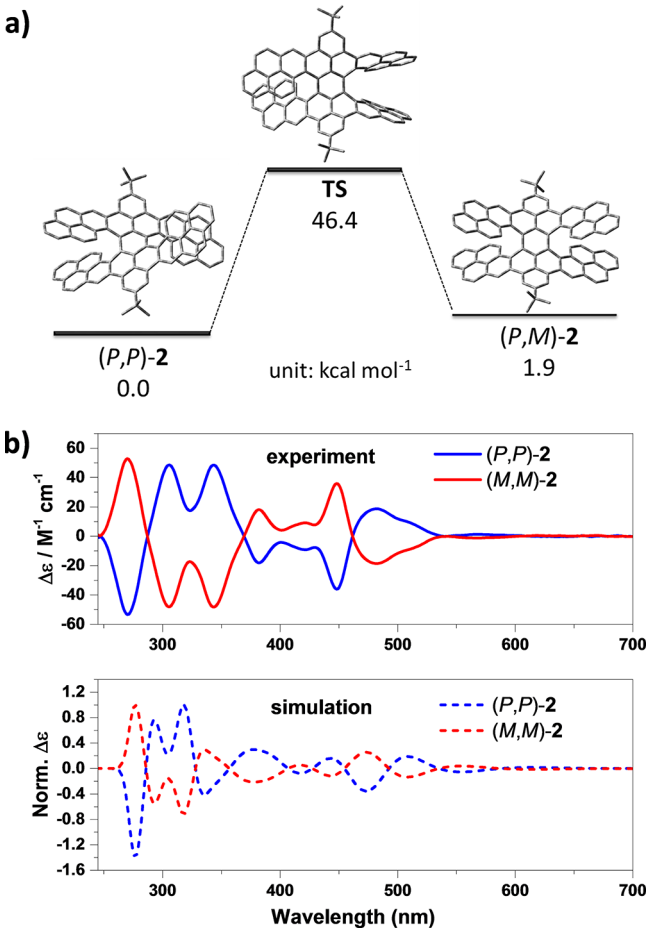

Figure 5. (a) Isomerization process between (*P*,*P*)-**2** and (*P*,*M*)-**2**. The relative Gibbs free energy was calculated at the B3LYP/6-311G(d,p) level. (b) Experimental and simulated circular dichroism spectra of (*P*,*P*)-**2** and (*M*,*M*)-**2**.

CONCLUSION

In summary, we have described the synthesis and characterizations of a π-extended double [7]carbohelicene **2**. In contrast to its smaller analogue **1**, **2** features a narrowed optical gap (ΔE_g = 0.35 eV) and significantly red-shifted emission ($\Delta\lambda_{em}$ = 162 nm) extending into the NIR region. Single-crystal X-ray analysis reveals significant overlaps at both helical ends in molecule **2** due to the extended π-conjugation. This considerable intramolecular $\pi-\pi$ interaction gives rise to the formation of a stabilized intramolecular excimer upon photoexcitation, as evidenced by the "excimer-like" emission and transient absorption spectroscopy. Remarkable intermolecular $\pi-\pi$ stacking has also been observed in crystals of **2**, hinting at its potential in (opto)electronic devices as a chiral semiconducting and light-emitting material. These results demonstrate the critical role of π-extension on the optoelectronic properties and crystal packing behavior of double helicenes, providing new perspectives in multihelicene chemistry.

EXPERIMENTAL SECTION

General Methods. All starting materials were purchased from Aldrich, Acros, and Alfa Aesar, and used as received without further purification. Preparative column chromatography was performed on silica gel from Merck with a grain size of 0.063−0.200 mm (silica gel). NMR spectra were recorded in CD_2Cl_2 on AVANCE 300 MHz or CD_2Cl_2/CS_2 (1/2) on AVANCE 500 MHz Bruker spectrometers. High-resolution mass spectrometry (HRMS) was performed on a SYNAPT G2 Si high-resolution time-of-flight mass spectrometer (Waters Corp., Manchester, UK) by matrix-assisted laser desorption/ionization (MALDI). Absorption spectra were recorded on a PerkinElmer Lambda 900 spectrophotometer. Fluorescence spectra were recorded on a J&MTIDAS spectrofluorometer. Cyclic voltammetry (CV) was performed on a WaveDriver 20 bipotentiostat/galvanostat (Pine Instruments Co.), and measurements were carried out in dichloromethane containing 0.1 M *n*-Bu_4NPF_6 as supporting electrolyte (scan rate: 100 mV s^{-1}). A glassy carbon electrode was used as a working electrode, a platinum wire as a counter electrode, and a silver wire as a reference electrode.

Synthesis of 2,2′,2″,2‴-(4,4″-Di-tert-butyl-[1,1′:4′,1″-terphenyl]-2,2″,6,6″-tetrayl)tetrapyrene (4). Under argon atmosphere, 2,2″,6,6″-tetrabromo-4,4″-di-*tert*-butyl-1,1′:4′,1″-terphenyl (**3**)[40] (102 mg, 0.155 mmol), 4,4,5,5-tetramethyl-2-(pyren-2-yl)-1,3,2-dioxaborolane[48] (305 mg, 0.929 mmol), tetrakis(triphenylphosphine)palladium(0) [$Pd(PPh_3)_4$] (23.0 mg, 0.0199 mmol), and potassium carbonate (K_2CO_3) (246 mg, 1.78 mmol) were dissolved in a degassed mixture of dioxane (18 mL) and water (2.7 mL). The resulting solution was heated to 100 °C and stirred at this temperature for 1 day. After being cooled to room temperature, the reaction mixture was diluted with water and extracted by dichloromethane. The organic phase was dried over anhydrous sodium sulfate and evaporated to dryness. The residue was purified via silica gel column chromatography with dichloromethane/hexane

DOI: 10.1021/jacs.9b05610
J. Am. Chem. Soc. 2019, 141, 12797−12803

(1/4) as eluent, and **4** was obtained as white powder (150 mg, 85% yield). ^{1}H NMR (300 MHz, CD_2Cl_2, 298 K, ppm) δ 8.12 (d, J = 7.6 Hz, 8H), 7.95 (t, J = 7.7 Hz, 4H), 7.82 (d, J = 8.9 Hz, 8H), 7.72 (s, 8H), 7.65 (d, J = 9.0 Hz, 8H), 7.34 (s, 4H), 6.31 (s, 4H), 1.23 (s, 18H); ^{13}C NMR (75 MHz, CD_2Cl_2, 298 K, ppm) δ 150.09, 142.08, 141.60, 135.57, 135.37, 131.72, 131.48, 130.88, 129.49, 127.75, 127.61, 127.03, 126.23, 125.31, 124.84, 123.36, 34.85, 31.38; HRMS (MALDI-TOF) m/z: calcd for $C_{90}H_{62}$, 1142.4852; found, 1142.4860 (M^+).

Synthesis of Pyrene-Fused Double [7]Carbohelicene **2**. Under argon atmosphere, compound **4** (50 mg, 0.044 mmol) and 2,3-dichloro-5,6-dicyano-1,4-benzoquinone (DDQ) (44 mg, 0.19 mmol) were dissolved in 25 mL of dry and degassed dichloromethane. The resulting solution was cooled to 0 °C, and triflic acid (0.025 mL) was then added dropwise. After further stirring at 0 °C for 2 h, the reaction mixture was neutralized by triethylamine, diluted with dichloromethane, and washed with water. The organic phase was dried over anhydrous sodium sulfate and evaporated to dryness. The residue was purified via silica gel column chromatography with dichlorometahne/hexane (1/2) as eluent, affording the title compound **2** as a brownish red solid (5.0 mg, 10%). ^{1}H NMR (500 MHz, $C_2D_2Cl_4$, 298 K, ppm) δ 9.62 (s, 4H), 9.52 (s, 4H), 8.11 (d, J = 8.6 Hz, 4H), 7.67 (d, J = 8.6 Hz, 4H), 7.57 (m, 16H), 6.95 (d, J = 8.9 Hz, 4H), 2.07 (s, 18H); ^{13}C NMR (75 MHz, $C_2D_2Cl_4$, 298 K, ppm) δ 192.98, 150.08, 131.44, 130.96, 130.17, 129.60, 129.10, 128.55, 127.15, 127.09, 125.73, 125.54, 125.37, 125.18, 124.76, 124.35, 123.73, 121.14, 119.49, 36.39, 32.65; HRMS (MALDI-TOF) m/z: calcd for $C_{90}H_{54}$, 1134.4226; found, 1134.4210 (M^+).

X-ray Crystallography. The single crystals of compound **2** suitable for X-ray analysis were obtained by diffusing hexane vapor into the carbon disulfide solution of **2**. The structure was deposited at The Cambridge Crystallographic Data Centre with a CCDC number of 1914718, and the data can be obtained free of charge via www.ccdc.cam.ac.uk/structures.

Transient Absorption Measurements. We used an amplified Ti:Sapphire laser with 2 mJ output energy, 1 kHz repetition rate, a pulse width of ∼150 fs, and a central energy of 800 nm. To excite compound **2** (0.1 mg/mL in THF and 0.05 mg/mL in polystyrene 40 mg/mL), we employed a pump wavelength of 530 nm with a spot diameter of 500 μm and a pump energy of 10 nJ. Such pump pulses were generated by using optical parameter amplification (OPA) in the visible range. As a probe pulse, we used a broadband white-light supercontinuum generated in a sapphire plate, extending from 450 to 780 nm. The pump−probe delay (up to 1 ns) was set by means of a mechanical stage.

■ ASSOCIATED CONTENT

Supporting Information

The Supporting Information is available free of charge on the ACS Publications website at DOI: 10.1021/jacs.9b05610.

Details of the X-ray single crystal analyses (Figure S1 and Table S1), theoretical calculations (Figures S2−S4 and Table S2), and optical resolution by chiral HPLC (Figure S7), as well as ^{1}H, ^{13}C NMR, and HRMS spectra (Figures S8−S14) (PDF)

X-ray crystallographic data (CIF)

X-ray crystallographic details (PDF)

■ AUTHOR INFORMATION

Corresponding Authors

*muellen@mpip-mainz.mpg.de

*narita@mpip-mainz.mpg.de

ORCID

Yunbin Hu: 0000-0001-5346-7059

Giuseppe M. Paternò: 0000-0003-2349-566X

Xiao-Ye Wang: 0000-0003-3540-0277

Xiao-Yu Cao: 0000-0003-0219-1798

Klaus Müllen: 0000-0001-6630-8786

Akimitsu Narita: 0000-0002-3625-522X

Notes

The authors declare no competing financial interest.

■ ACKNOWLEDGMENTS

This work was financially supported by the Max Planck Society and the European Commission Graphene Flagship Core1 under Horizon 2020 (project ID: 696656). G.M.P. was supported by the EU Horizon 2020 Research and Innovation Program (grant agreement 643238 (SYNCHRONICS)). F.S. acknowledges support from the European Research Council (ERC) under the European Union's Horizon 2020 research and innovation program (grant agreement no. [816313]). Y.H. acknowledges support from a research start-up fund (202045007) and innovation driven program (502501009) of Central South University. We thank Steven D. Aird for editing the manuscript.

■ REFERENCES

(1) Narita, A.; Wang, X.-Y.; Feng, X.; Müllen, K. New advances in nanographene chemistry. *Chem. Soc. Rev.* **2015**, *44*, 6616−6643.

(2) Ball, M.; Zhong, Y.; Wu, Y.; Schenck, C.; Ng, F.; Steigerwald, M.; Xiao, S.; Nuckolls, C. Contorted polycyclic aromatics. *Acc. Chem. Res.* **2015**, *48*, 267−276.

(3) Pun, S. H.; Miao, Q. Toward Negatively Curved Carbons. *Acc. Chem. Res.* **2018**, *51*, 1630−1642.

(4) Márquez, I. R.; Castro-Fernández, S.; Millán, A.; Campaña, A. G. Synthesis of distorted nanographenes containing seven- and eight-membered carbocycles. *Chem. Commun.* **2018**, *54*, 6705−6718.

(5) Rickhaus, M.; Mayor, M.; Juricek, M. Chirality in curved polyaromatic systems. *Chem. Soc. Rev.* **2017**, *46*, 1643−1660.

(6) Yang, W.; Longhi, G.; Abbate, S.; Lucote, A.; Tommasini, M.; Villani, C.; Catalano, V. J.; Lykhin, A. O.; Varganov, S. A.; Chalifoux, W. A. Chiral Peropyrene: Synthesis, Structure, and Properties. *J. Am. Chem. Soc.* **2017**, *139*, 13102−13109.

(7) Kawai, K.; Kato, K.; Peng, L.; Segawa, Y.; Scott, L. T.; Itami, K. Synthesis and Structure of a Propeller-Shaped Polycyclic Aromatic Hydrocarbon Containing Seven-Membered Rings. *Org. Lett.* **2018**, *20*, 1932−1935.

(8) Zhu, Y.; Xia, Z.; Cai, Z.; Yuan, Z.; Jiang, N.; Li, T.; Wang, Y.; Guo, X.; Li, Z.; Ma, S.; Zhong, D.; Li, Y.; Wang, J. Synthesis and characterization of hexapole [7]helicene, a circularly twisted chiral nanographene. *J. Am. Chem. Soc.* **2018**, *140*, 4222−4226.

(9) Berezhnaia, V.; Roy, M.; Vanthuyne, N.; Villa, M.; Naubron, J. V.; Rodriguez, J.; Coquerel, Y.; Gingras, M. Chiral nanographene propeller embedding six enantiomerically stable [5]helicene units. *J. Am. Chem. Soc.* **2017**, *139*, 18508−18511.

(10) Malik, A. U.; Gan, F.; Shen, C.; Yu, N.; Wang, R.; Crassous, J.; Shu, M.; Qiu, H. Chiral Organic Cages with a Triple-Stranded Helical Structure Derived from Helicene. *J. Am. Chem. Soc.* **2018**, *140*, 6510−6510.

(11) Heffern, M. C.; Matosziuk, L. M.; Meade, T. J. Lanthanide Probes for Bioresponsive Imaging. *Chem. Rev.* **2014**, *114*, 4496−4539.

(12) Yuan, L.; Lin, W.; Zheng, K.; He, L.; Huang, W. Far-red to near infrared analyte-responsive fluorescent probes based on organic fluorophore platforms for fluorescence imaging. *Chem. Soc. Rev.* **2013**, *42*, 622−661.

(13) Xue, J.; Liang, Q.; Zhang, Y.; Zhang, R.; Duan, L.; Qiao, J. High-Efficiency Near-Infrared Fluorescent Organic Light-Emitting Diodes with Small Efficiency Roll-Off: A Combined Design from Emitters to Devices. *Adv. Funct. Mater.* **2017**, *27*, 1703283.

(14) Wang, S.; Yan, X.; Cheng, Z.; Zhang, H.; Liu, Y.; Wang, Y. Highly Efficient Near-Infrared Delayed Fluorescence Organic Light

Emitting Diodes Using a Phenanthrene-Based Charge-Transfer. *Angew. Chem., Int. Ed.* **2015**, *54*, 13068−13072.
(15) Yang, Y.; Correa da Costa, R.; Fuchter, M. J.; Campbell, A. J. Circularly polarized light detection by a chiral organic semiconductor transistor. *Nat. Photonics* **2013**, *7*, 634−638.
(16) Brédas, J.-L.; Beljonne, D.; Coropceanu, V.; Cornil, J. Charge-Transfer and Energy-Transfer Processes in π-Conjugated Oligomers and Polymers: A Molecular Picture. *Chem. Rev.* **2004**, *104*, 4971−5004.
(17) Chen, Z.; Lohr, A.; Saha-Möller, C. R.; Würthner, F. Self-assembled π-stacks of functional dyes in solution: structural and thermodynamic features. *Chem. Soc. Rev.* **2009**, *38*, 564−584.
(18) Saeki, A.; Koizumi, Y.; Aida, T.; Seki, S. Comprehensive Approach to Intrinsic Charge Carrier Mobility in Conjugated Organic Molecules, Macromolecules, and Supramolecular Architectures. *Acc. Chem. Res.* **2012**, *45*, 1193−1202.
(19) Shan, L.; Liu, D.; Li, H.; Xu, X.; Shan, B.; Xu, J.-B.; Miao, Q. Monolayer Field-Effect Transistors of Nonplanar Organic Semiconductors with Brickwork Arrangement. *Adv. Mater.* **2015**, *27*, 3418−3423.
(20) Matsuoka, W.; Ito, H.; Itami, K. Rapid Access to Nanographenes and Fused Heteroaromatics by Palladium-Catalyzed Annulative π-Extension Reaction of Unfunctionalized Aromatics with Diiodobiaryls. *Angew. Chem., Int. Ed.* **2017**, *56*, 12224−12228.
(21) Pola, S.; Kuo, C.-H.; Peng, W.-T.; Islam, Md. M.; Chao, I.; Tao, Y.-T. Contorted Tetrabenzocoronene Derivatives for Single Crystal Field Effect Transistors: Correlation between Packing and Mobility. *Chem. Mater.* **2012**, *24*, 2566−2571.
(22) Gingras, M. One hundred years of helicene chemistry. Part 3: applications and properties of carbohelicenes. *Chem. Soc. Rev.* **2013**, *42*, 1051−1095.
(23) Gingras, M. One hundred years of helicene chemistry. Part 1: non-stereoselective syntheses of carbohelicenes. *Chem. Soc. Rev.* **2013**, *42*, 968−1006.
(24) Gingras, M.; Felix, G.; Peresutti, R. One hundred years of helicene chemistry. Part 2: stereoselective syntheses and chiral separations of carbohelicenes. *Chem. Soc. Rev.* **2013**, *42*, 1007−1050.
(25) Urbano, A.; Carreno, M. C. Enantioselective synthesis of helicenequinones and − bisquinones. *Org. Biomol. Chem.* **2013**, *11*, 699−708.
(26) Mori, K.; Murase, T.; Fujita, M. One-Step Synthesis of [16]Helicene. *Angew. Chem., Int. Ed.* **2015**, *54*, 6847−6851.
(27) Clar, E.; Stewart, D. G. Aromatic Hydrocarbons. LXIII. Resonance Restriction and the Absorption Spectra of Aromatic Hydrocarbons. *J. Am. Chem. Soc.* **1952**, *74*, 6235−6238.
(28) Newman, M. S.; Lednicer, D. The Synthesis and Resolution of Hexahelicene. *J. Am. Chem. Soc.* **1956**, *78*, 4765−4770.
(29) Flammang-Barbieux, M.; Nasielski, J.; Martin, R. H. Synthesis of heptahelicene (1) benzo [c] phenanthro [4, 3-g]phenanthrene. *Tetrahedron Lett.* **1967**, *8*, 743−744.
(30) Martin, R. H.; Flammang-Barbieux, M.; Cosyn, J. P.; Gelbcke, M. 1-Synthesis of octa- and nonahelicenes. 2-New syntheses of hexa- and heptahelicenes. 3-Optical rotation and O.R.D. of heptahelicene. *Tetrahedron Lett.* **1968**, *9*, 3507−3510.
(31) Buchta, M.; Rybáček, J.; Jančařík, A.; Kudale, A. A.; Buděšínský, M.; Chocholoušová, J. V.; Vacek, J.; Bednárová, L.; Císařová, I.; Bodwell, G. J.; Starý, I.; Stará, I. G. Chimerical Pyrene-Based [7]Helicenes as Twisted Polycondensed Aromatics. *Chem. - Eur. J.* **2015**, *21*, 8910−8917.
(32) Nakakuki, Y.; Hirose, T.; Sotome, H.; Miyasaka, H.; Matsuda, K. Hexa-peri-hexabenzo [7]helicene: Homogeneously pi-Extended Helicene as a Primary Substructure of Helically Twisted Chiral Graphenes. *J. Am. Chem. Soc.* **2018**, *140*, 4317−4326.
(33) Cruz, C. M.; Castro-Fernández, S.; Maçôas, E.; Cuerva, J. M.; Campaña, A. G. Undecabenzo[7]superhelicene: A Helical Nanographene Ribbon as a Circularly Polarized Luminescence Emitter. *Angew. Chem., Int. Ed.* **2018**, *57*, 14782−14786.
(34) Evans, P. J.; Ouyang, J.; Favereau, L.; Crassous, J.; Fernández, I.; Perles, J.; Martín, N. Synthesis of a Helical Bilayer Nanographene. *Angew. Chem., Int. Ed.* **2018**, *57*, 6774−6779.
(35) Li, C.; Yang, Y.; Miao, Q. Recent Progress in Chemistry of Multiple Helicenes. *Chem. - Asian J.* **2018**, *13*, 884−894.
(36) Fujikawa, T.; Segawa, Y.; Itami, K. Synthesis, Structures, and Properties of pi-Extended Double Helicene: A Combination of Planar and Nonplanar pi-Systems. *J. Am. Chem. Soc.* **2015**, *137*, 7763−7768.
(37) Yanney, M.; Fronczek, F. R.; Henry, W. P.; Beard, D. J.; Sygula, A. Cyclotrimerization of Corannulyne: Steric Hindrance Tunes the Inversion Barriers of Corannulene Bowls. *Eur. J. Org. Chem.* **2011**, *2011*, 6636−6639.
(38) Zhu, Y.; Xia, Z.; Cai, Z.; Yuan, Z.; Jiang, N.; Li, T.; Wang, Y.; Guo, X.; Li, Z.; Ma, S.; Zhong, D.; Li, Y.; Wang, J. Synthesis and Characterization of Hexapole [7]Helicene, A Circularly Twisted Chiral Nanographene. *J. Am. Chem. Soc.* **2018**, *140*, 4222−4226.
(39) Wang, Y.; Yin, Z.; Zhu, Y.; Gu, J.; Li, Y.; Wang, J. Hexapole [9]Helicene. *Angew. Chem., Int. Ed.* **2019**, *58*, 587−591.
(40) Hu, Y.; Wang, X.-Y.; Peng, P.-X.; Wang, X.-C.; Cao, X.-Y.; Feng, X.; Müllen, K.; Narita, A. Benzo-Fused Double [7]-Carbohelicene: Synthesis, Structures, and Physicochemical Properties. *Angew. Chem., Int. Ed.* **2017**, *56*, 3374−3378.
(41) Goddard, R.; Haenel, M. W.; Herndon, W. C.; Kruger, C.; Zander, M. Crystallization of Large Planar Polycyclic Aromatic Hydrocarbons: The Molecular and Crystal Structures of Hexabenzo-[bc,ef,hi,kl,no,qr]coronene and Benzo[1,2,3-bc:4,5,6-b'c']dicoronene. *J. Am. Chem. Soc.* **1995**, *117*, 30−41.
(42) Luo, J.; Xu, X.; Mao, R.; Miao, Q. Curved Polycyclic Aromatic Molecules That Are π-Isoelectronic to Hexabenzocoronene. *J. Am. Chem. Soc.* **2012**, *134*, 13796−13803.
(43) Paterno, G. M.; Chen, Q.; Wang, X.-Y.; Liu, J.; Motti, S. G.; Petrozza, A.; Feng, X.; Lanzani, G.; Müllen, K.; Narita, A.; Scotognella, F. Synthesis of Dibenzo[hi,st]ovalene and Its Amplified Spontaneous Emission in a Polystyrene Matrix. *Angew. Chem., Int. Ed.* **2017**, *56*, 6753−6757.
(44) Paternò, G. M.; Nicoli, L.; Chen, Q.; Müllen, K.; Narita, A.; Lanzani, G.; Scotognella, F. Modulation of the Nonlinear Optical Properties of Dibenzo[hi,st]ovalene by Peripheral Substituents. *J. Phys. Chem. C* **2018**, *122*, 25007−25013.
(45) Paternò, G. M.; Moretti, L.; Barker, A. J.; Chen, Q.; Müllen, K.; Narita, A.; Cerullo, G.; Scotognella, F.; Lanzani, G. Pump−Push−Probe for Ultrafast All-Optical Switching: The Case of a Nanographene Molecule. *Adv. Funct. Mater.* **2019**, *29*, 1805249.
(46) Brown, K. E.; Salamant, W. A.; Shoer, L. E.; Young, R. M.; Wasielewski, M. R. Direct Observation of Ultrafast Excimer Formation in Covalent Perylenediimide Dimers Using Near-Infrared Transient Absorption Spectroscopy. *J. Phys. Chem. Lett.* **2014**, *5*, 2588−2593.
(47) Giaimo, J. M.; Lockard, J. V.; Sinks, L. E.; Scott, A. M.; Wilson, T. M.; Wasielewski, M. R. Excited Singlet States of Covalently Bound, Cofacial Dimers and Trimers of Perylene-3,4:9,10-bis-(dicarboximide)s. *J. Phys. Chem. A* **2008**, *112*, 2322−2330.
(48) Oniwa, K.; Kikuchi, H.; Shimotani, H.; Ikeda, S.; Asao, N.; Yamamoto, Y.; Tanigaki, K.; Jin, T. 2-Positional pyrene end-capped oligothiophenes for high performance organic field effect transistors. *Chem. Commun.* **2016**, *52*, 4800−4803.

DOI: 10.1021/jacs.9b05610
J. Am. Chem. Soc. 2019, 141, 12797−12803